ACSNANO
www.acsnano.org
ARTICLE

Colloidal Spherical Quantum Wells with Near-Unity Photoluminescence Quantum Yield and Suppressed Blinking

Byeong Guk Jeong,[†] Young-Shin Park,[‡,§] Jun Hyuk Chang,[⊥] Ikjun Cho,[∥] Jai Kyeong Kim,[¶] Heesuk Kim,[¶] Kookheon Char,[⊥] Jinhan Cho,[∥] Victor I. Klimov,[‡] Philip Park,[*,#] Doh C. Lee,[*,†] and Wan Ki Bae[*,¶]

[†]Department of Chemical and Biomolecular Engineering, KAIST Institute for the Nanocentury, Korea Advanced Institute of Science and Technology (KAIST), 291 Daehak-ro, Yuseong-gu, Daejeon 34141, Republic of Korea

[‡]Chemistry Division, Los Alamos National Laboratory, Los Alamos, New Mexico 87545, United States

[§]Center for High Technology Materials, University of New Mexico, Albuquerque, New Mexico 87131, United States

[⊥]School of Chemical and Biological Engineering, The National Creative Research Initiative Center for Intelligent Hybrids, Seoul National University, 1 Gwanak-ro, Gwanak-gu, Seoul 08826, Republic of Korea

[∥]Department of Chemical and Biological Engineering, Korea University, 145 Anam-ro, Seongbuk-gu, Seoul 02841, Republic of Korea

[¶]Photoelectronic Hybrids Research Center, Korea Institute of Science and Technology (KIST), 14-gil 5 Hwarang-ro, Seongbuk-gu, Seoul 02792, Republic of Korea

[#]Department of Chemistry and Biochemistry, University of California, Los Angeles, California 90095, United States

Supporting Information

ABSTRACT: **Thick inorganic shells endow colloidal nanocrystals (NCs) with enhanced photochemical stability and suppression of photoluminescence intermittency (also known as blinking). However, the progress of using thick-shell heterostructure NCs in applications has been limited due to the low photoluminescence quantum yield (PL QY ≤ 60%) at room temperature. Here, we demonstrate thick-shell NCs with CdS/CdSe/CdS seed/spherical quantum well/shell (SQW) geometry that exhibit near-unity PL QY at room temperature and suppression of blinking. In SQW NCs, the lattice mismatch is diminished between the emissive CdSe layer and the surrounding CdS layers as a result of coherent strain, which suppresses the formation of misfit defects and consequently permits ∼100% PL QY for SQW NCs with a thick CdS shell (≥5 nm). High PL QY of thick-shell SQW NCs is preserved even in concentrated dispersion and in film under thermal stress, which makes them promising candidates for applications in solid-state lightings and luminescent solar concentrators.**

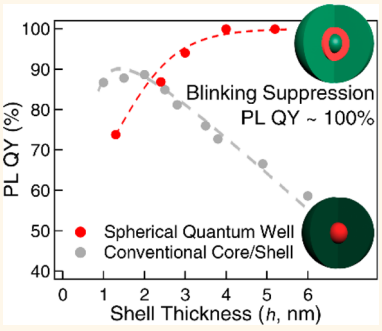

KEYWORDS: *spherical quantum well, near-unity photoluminescence quantum yield, coherently strained heterostructure, misfit defect, critical thickness*

Colloidal semiconductor nanocrystals (NCs) exhibit narrow spectral emission bandwidth and high photoluminescence quantum yield (PL QY),[1] calling attention to their use in displays,[2−10] lasers,[11−13] and luminescent solar concentrators (LSCs).[14−17] Synthesis of high-quality colloidal NCs suitable for such applications has become possible *via* "arrested precipitation", in which organic ligands bind to the surface of NCs and confer size tunability and solution processability.[18] However, the relatively weak bonding between organic ligands and surface atoms of NCs yields low PL QY and unavoidable degradation of optical properties of NCs.[19]

Coating an emitting core with an inorganic semiconductor shell of a wider band gap can result in higher PL QYs and improved photochemical stability of the NCs,[20] which has motivated the development of core/shell (C/S) heterostructured NCs with thick-shell layers.[5,8,21−25] In addition to reducing the influence of surface-related nonradiative recombination pathways,[21,22] the thick shells help impede energy transfer between neighboring NCs by separating the emitting cores in concentrated NC ensembles.[8,17] The latter is important for maintaining high PL QYs in dense, device-grade QD films, as energy transfer occurs more readily between NCs within the

Received: June 6, 2016
Accepted: October 2, 2016
Published: October 2, 2016

DOI: 10.1021/acsnano.6b03704
ACS Nano 2016, 10, 9297−9305

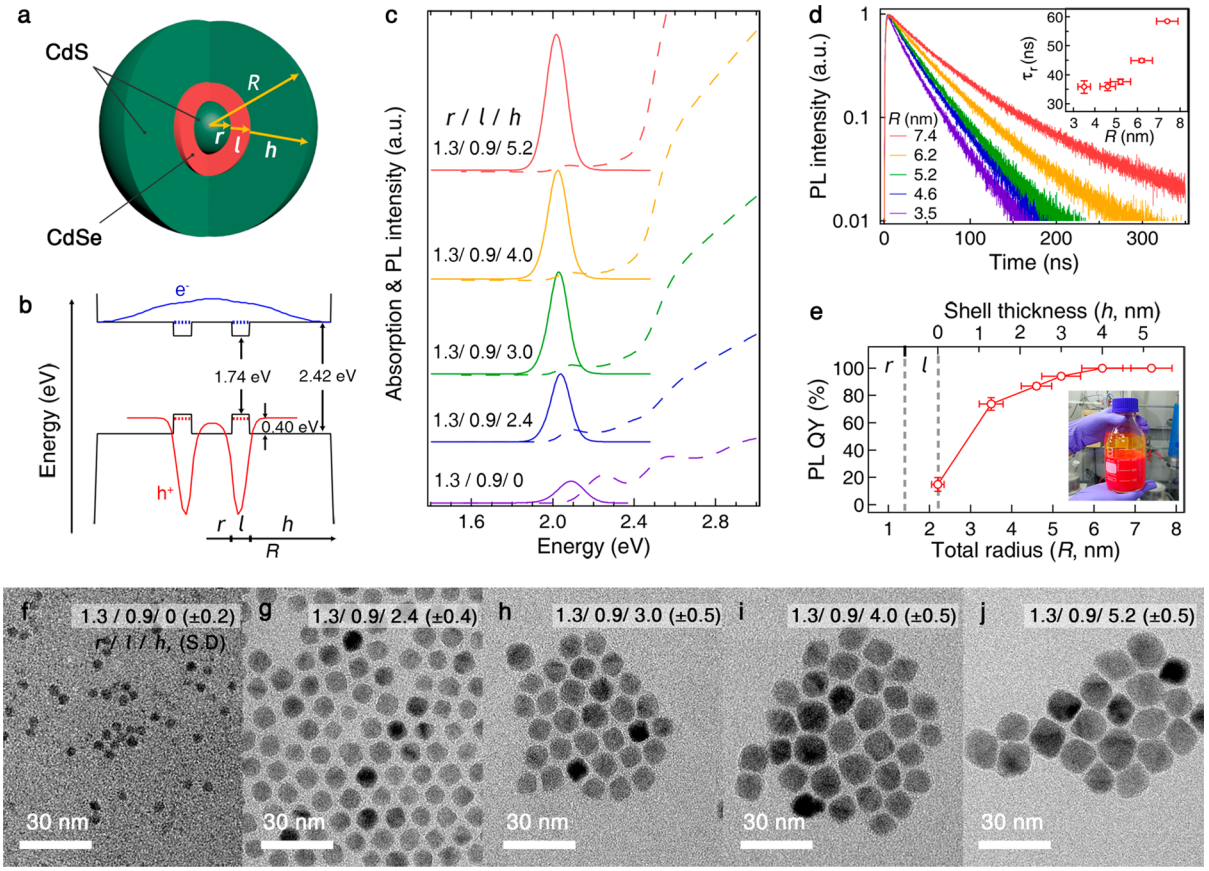

Figure 1. Structural and optical characteristics of CdS/CdSe/CdS SQW NCs with varying shell thicknesses. (a) Schematic illustration and (b) energy band diagram of CdS/CdSe/CdS SQW NCs. *r*, *l*, *h*, and *R* denote the radius of the CdS seed, the thickness of the CdSe emissive layer, the exterior CdS shell thickness, and the total radius, respectively. (c) Absorption and PL spectra, (d) ensemble PL decay dynamics (inset: single-exciton radiative recombination lifetime (τ_r)), (e) PL QYs excited at 450 nm (inset: photograph of concentrated SQW NC dispersion (300 mg/mL) taken under room light), and (f–j) TEM images of CdS/CdSe/CdS SQW NCs with varying CdS shell thicknesses (*r* = 1.3 nm, *l* = 0.9 nm, *h* = 0, 2.4, 3.0, 4.0, and 5.2 nm).

exciton-transfer distance.[8] Furthermore, in the case of mixed-size NC assemblies, energy transfer may result in the undesired cross-talk between the NCs, leading to changes in the color pattern. One notable example of thick-shell structures are so-called "giant" NCs that comprise a small CdSe core overcoated with a very thick (≥5 nm) CdS shell.[24−30] The original motivation for the development of these NCs was to achieve the suppression of single-dot PL intermittency (commonly referred to as "blinking").[24,26] Eventually, it was demonstrated that these structures also allow for considerable suppression of nonradiative Auger recombination and interparticle exciton transfer.[23,25,28−30] An important feature of giant NCs is a vast enhancement of environment, chemical, thermal, and photochemical stability as compared to standard core-only or thin-shell NCs.[17,26]

Despite promising properties of thick-shell heterostructured NCs, their use in light-emitting applications has been hampered by fairly low room-temperature PL QYs. For example, PL QY of CdSe/CdS giant C/S NCs is at least 40% lower than that of thin-shell CdSe/CdS C/S NCs (Figure S1, Supporting Information).[23−26,30−33] The PL QY loss in giant C/S NCs has been attributed to the formation of interfacial defect sites driven by increasing crystalline strain between the core and the shell.[34] Insertion of alloyed layers at the core/shell interface has been proposed to help mitigate the structural stress[34] and enhance PL efficiency of thick-shell C/S NCs.[35] However, thick-shell C/S NCs have shown PL QY lower than 60% even in the case of structures with alloyed core/shell interfaces.[34,35]

In the present study, we demonstrate a coherently strained heterostructure that capitalizes on the structural deformation of emissive layers to alleviate the structural stress upon growing a thick shell. We designed CdS/CdSe/CdS seed/spherical quantum well/shell (hereafter, SQW) NCs, in which the intermediate CdSe layer is expected to grow *via* strained layer epitaxy. A comparison with conventional CdSe/CdS C/S NCs reveals that the misfit defects responsible for the PL QY loss in thick-shell C/S NCs do not appear in SQW NCs with thick shells (*e.g.*, shell thickness ≥5 nm). Our giant SQW NCs exhibit a nearly 100% PL QY at room temperature and, at the same time, substantial suppression of PL blinking. In addition, systematic investigation on SQW NCs with varying geometric parameters (*e.g.*, CdS seed radius, volume of CdSe emissive layer, and CdS shell thickness) not only provides insights into the relationship between the structure of the SQW NCs and their optical properties but also validates the proposed model of the effect of SQW heterostructuring on the optical performance of the NCs. Finally, we examine the emission characteristics of giant SQW NCs in comparison with state-of-the-art C/S NCs in highly concentrated suspensions and films. The superior optical properties and thermal stability render SQW NCs suitable for use in solid-state lightings and LSCs.

DOI: 10.1021/acsnano.6b03704
ACS Nano 2016, 10, 9297−9305

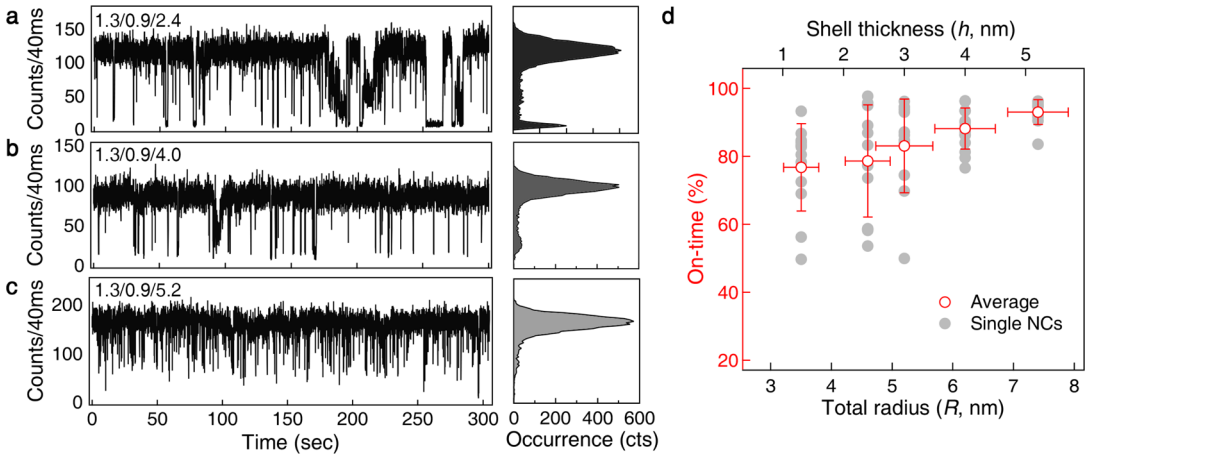

Figure 2. Single-dot spectroscopic characteristics of CdS/CdSe/CdS SQW NCs with varying shell thicknesses. (a–c) **Representative PL intensity trajectories (left) and PL intensity histograms (right) of CdS (r = 1.3 nm)/CdSe (l = 0.9 nm)/CdS SQW NCs with varying shell thicknesses (h = (a) 2.4, (b) 4.0, and (c) 5.2 nm). (d) The ON-time fraction for single NCs of CdS/CdSe/CdS SQWs with different shell thicknesses (r = 1.3 nm, l = 0.9 nm, h = 1.3, 2.4, 3.0, 4.0, and 5.2 nm).**

RESULTS AND DISCUSSION

The concept of coherently strained multilayered heterostructures proposed by Matthews and Blakeslee entails the relaxation of crystalline strain at an interface,[36] where one crystal structure is deformed to fit the structure of an adjacent crystal. We employ the coherently strained layer approach by growing a CdSe layer sandwiched between the CdS core NC and CdS shell. Heterostructured NCs composed of zinc blende CdSe and CdS are chosen as a model system for two reasons: (i) The chemistry to grow these compound semiconductors is well-established,[27,31,37] and (ii) the photophysical properties of heterostructured NCs (*e.g.*, CdSe/CdS C/S NCs) have been extensively studied.[23−33,35,38−41] We designed CdS/CdSe/CdS SQW NCs,[37] in which a thin CdSe layer (thickness ≤1.5 nm) forms on the surface of the CdS seed, which is followed by growth of a CdS shell (Figure 1a). The preparation of CdSe and CdS layers was carried out under reaction conditions (*i.e.*, identities of precursors and ligands, reaction temperature, and duration) that were similar to those used in the synthesis of conventional CdSe/CdS C/S NCs (Supporting Information).[31] Therefore, we expect that the surface atom stoichiometry and ligand density in both types of the NCs are similar. Both C/S and SQW NCs possess a quasi-type-II band alignment (Figure 1b), in which a hole is strongly confined within the CdSe emissive layer, whereas an electron is delocalized over the entire nanostructure volume. The electron confinement energy reduces with increasing exterior CdS shell thickness, resulting in the red shift of the 1S band-edge absorption and the PL peak position (Figure 1c).[23,24,27,31] The decrease in the electron−hole overlap integral with increasing CdS shell thickness results in a progressive reduction of the single-exciton recombination rate (Figure 1d).[23,24,27,31] Despite similarity in optical properties (*i.e.*, similar PL energies and single-exciton lifetimes), the size dependence of PL QY in the case of SQW NCs considerably differs from that of C/S NCs. Namely, in the case of C/S NCs, PL QY first increases with increasing CdS shell thickness, but then it tapers off as the shell thickness becomes greater than 2.0 nm (Figure S1, Supporting Information).[31,33,34] In contrast, the PL QY of SQW NCs shows a continuous increase with increasing thickness of the CdS shell and eventually approaches 100% at thicknesses greater than 4 nm (Figure 1e; see also Supporting Information). Multiple independent runs confirm that the PL QY of SQW NCs is consistent batch-to-batch (Experimental Methods).

We have conducted spectroscopic analysis on individual SQW NCs (Figure 2). Figure 2a–c displays a representative PL intensity trajectory and corresponding histogram of PL intensities during the high- (ON) and low- (OFF) emissivity periods for SQW NCs at various CdS shell thicknesses. The PL intensity of thin-shell SQW NCs fluctuates between two well-defined ON and OFF levels, as is also apparent from the histogram in Figure 2a. The overall duration of the OFF periods decreases as the CdS shell thickness increases (Figure 2b), and the OFF periods almost completely disappear (*i.e.*, NC becomes "nonblinking") for shell thicknesses greater than 5 nm (Figure 2c). Interestingly, at sufficiently large shell thicknesses, a virtually non-emitting OFF state turns into a weakly emitting "gray" state. A similar transformation has been previously observed for thick-shell C/S NCs.[24,27,30] This transformation has been attributed to suppressed Auger recombination, which increases the PL QY of negative trions, the species with which the OFF state has often been associated.[24,29,30,42,43] The average ON-time fraction of thick-shell SQW samples shows a size dependence trend that is similar to that observed for PL QYs of solution samples (Figure 2d). This indicates that the PL blinking observed for individual NCs and the PL QY loss in ensemble samples are related phenomena, as suggested by the studies of ref 44.

In contrast to the case of SQW NCs, conventional CdSe/CdS giant NCs (shell thickness ≥ 16 CdS monolayers (MLs)) are reported to exhibit blinking suppression in single-dot spectroscopic measurements, yet with relatively low solution PL QY at room temperature (≤60%).[24−26,28−30] The conflict creates obscurity in the influence of thick shells on the photophysical properties of NCs. We speculate that the disparity in the case of traditional C/S thick-shell samples originates from the presence of non-emissive (or low-emissivity) NCs, which may not be detected in single-dot spectroscopic studies while contributing to the ensemble PL QY measurements.

As the shell thickness increases in C/S geometry, the CdS crystal in the shell, which is initially deformed to fit to the lattice constant of CdSe seed (zinc blende a_0 = 0.608 nm),

DOI: 10.1021/acsnano.6b03704
ACS Nano 2016, 10, 9297−9305

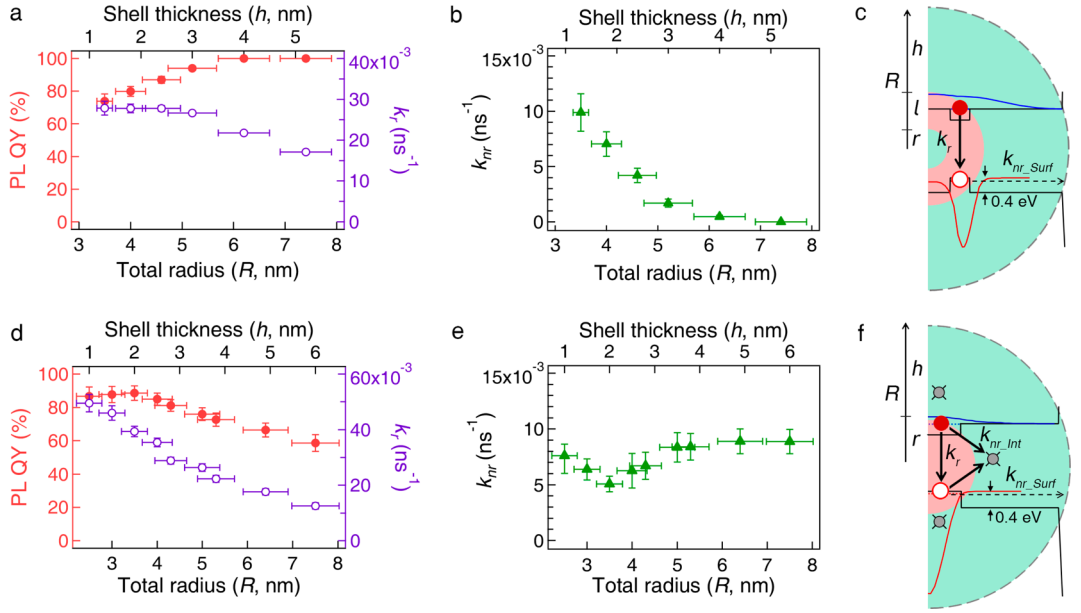

Figure 3. Exciton recombination pathways in CdS/CdSe/CdS SQW NCs and CdSe/CdS C/S NCs. (a,d) PL QYs (filled) and radiative exciton recombination rates (empty); (b,e) nonradiative recombination rates (triangles); and (c,f) schematic illustration for exciton recombination processes in (a−c) CdS/CdSe/CdS SQW NCs having different shell thicknesses (r = 1.3 nm, l = 0.9 nm, 1.3 ≤ h ≤ 5.2 nm) and (d−f) CdSe/CdS C/S NCs with varying shell thicknesses (r = 1.5 nm, 1 ≤ h ≤ 6.0 nm). All spectroscopic data were collected from SQW ensemble samples in solution.

starts to relax to its equilibrium lattice constant (zinc blende a_0 = 0.582 nm), leading to the formation of misfit defects (Figure 3 and Supporting Information).[34] The dangling bonds in misfit defects are effective charge-trapping sites, which are responsible for the presence of non-emissive (or low-emissivity) NCs and account for PL losses in giant C/S NCs.[45,46]

To gain a deeper insight into the role of interfacial defects in carrier recombination, we have attempted to quantify their contribution to the overall nonradiative decay rate in NCs with various shell thicknesses. The PL QY of NCs is given by

$$\text{PL QY} = k_r/(k_r + k_{nr}) \quad (1)$$

where k_r and k_{nr} denote the rates of radiative and nonradiative recombination of the exciton state, respectively. We would like to point out that the simplified expression for the PL QY given by eq 1 does not account for either possible presence of nonemissive NCs or occurrence of OFF periods in single-dot PL intensity trajectories. Nevertheless, as we show below, it presents interesting qualitative insights into the shell-thickness dependence of PL QYs in traditional C/S quantum dots versus that the novel SQW NCs.

Since PL QY of SQW NCs becomes higher as the shell grows thicker and reaches almost 100% at the shell thickness equal to or greater than 4 nm, we can assume that the influence of surface defects becomes vanishingly small in thick-shell SQW NCs (Figure 3b). This also suggests the absence of defects associated with two internal (CdS/CdSe and CdSe/CdS) interfaces across the entire range of h. Thus, nonradiative recombination in the case of small and intermediate shell thicknesses in SQW NCs can be presented as being solely due to surface defects. We further assume that the main channel for nonradiative decay is hole trapping at surface defects, associated with, for example, S dangling bonds or other imperfections on the surface of the CdS shell.[47,48] Since the surface properties and the CdSe/CdS valence band offset are similar between the C/S and SQW NCs, the trends of k_{nr} derived from the measurements of the SQW samples are likely valid in the case of the C/S structures.

To find the influence of a nonradiative pathway *via* misfit defects in C/S NCs, we use the plot of k_{nr} *versus* shell thicknesses (Figure 3e). Initially, the increase in h leads to the reduction of the nonradiative decay rate (accompanied by the PL QY increase; Figure 3d), which is likely a result of reduced trapping at surface defect (k_{nr_surf}), as in the case of the SQW NCs. However, when the shell thickness reaches approximately 2.5 nm, the trend reverses; that is, a further increase in h leads to the increased nonradiative rate accompanied by the reduction of the PL QY (Figure 3d,e). This can be interpreted as the onset of the formation of interfacial defects that help relax the lattice mismatch between the CdSe core and the CdS shell. Indeed, the onset shell thickness of 2.5 nm obtained in this study is in good agreement with previous experimental observations[33,34] as well as the estimation of the critical thickness for the formation of misfit defects (*ca.* 3.3 nm; see Supporting Information) based on Matthews and Blakeslee's equilibrium theory.[36,49,50]

In the case of C/S NCs, a thin CdS shell layer deforms its crystalline structure to minimize the structural stress at the CdSe/CdS interface. The energy that it takes to strain the CdS lattice increases as the shell continues to grow thicker and eventually exceeds the energy required to form misfit defects. Such disparity leads to the relaxation of the CdS crystal to its equilibrium lattice constant by forming misfit defects near the interface.[34] The rate of nonradiative decay *via* misfit defects (k_{nr_Int}) may rise at a thickness greater than the critical value and accelerates overall nonradiative recombination. As a result, the PL QY of C/S NCs starts to decline as the shell thickness increases. On the other hand, in the case of SQW NCs, the CdSe emissive layer is thinner than the critical thickness (*ca.* 3.6 nm; see Supporting Information), and thus the layer remains coherently strained, which hinders the formation of misfit defects. The fact that in the SQW structures the CdSe is in a

DOI: 10.1021/acsnano.6b03704
ACS Nano 2016, 10, 9297−9305

"strained" state is confirmed by X-ray diffraction (XRD) studies of the SQW and CdSe NCs (Figure 4).

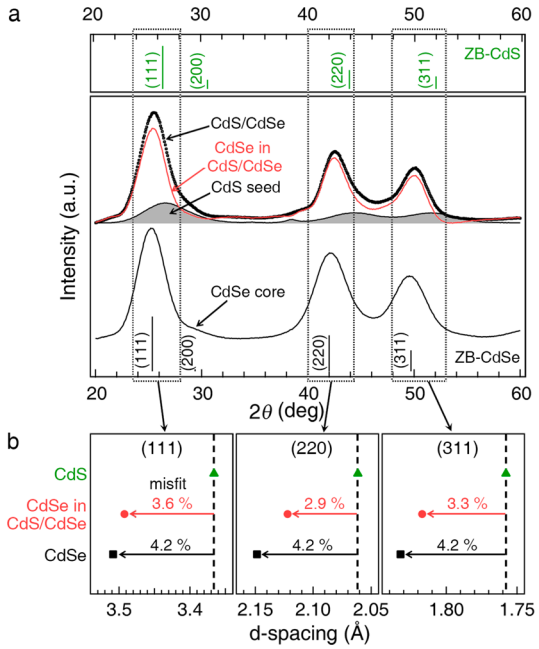

Figure 4. XRD patterns of CdSe spherical quantum well and CdSe core NCs. (a) XRD patterns of CdSe NCs (r = 1.5 nm, black solid) and CdS/CdSe NCs (r = 1.3 nm, l = 0.9 nm, empty circle). For SQW NCs, each (111), (220), and (311) peak is deconvoluted into peaks contributed from the CdSe emissive layer (red line) and CdS seed (gray shading). XRD patterns of bulk zinc blende CdSe (bottom) and CdS (top) are shown for comparison. (b) d-Spacing for (111), (220), and (311) planes of CdSe core (black square), CdSe SQW (red circle), and CdS (green triangle). Numbers represent lattice mismatch between CdSe and bulk CdS for the case of SQW (red) and CdSe NCs (black).

Specifically, according to the measured XRD patterns, the mismatch between the CdS lattice and the lattice of CdSe intermediate layer in the SQW NCs is ~3.3%, which is considerably smaller than the bulk lattice value of 4.2%. The deformed CdSe emissive layer alleviates the structural strain in the lattice of the exterior CdS layer, which suppresses the formation of misfit defects even for CdS shells thicker than 5 nm. All in all, because of the relieved strain, the nonradiative decay *via* interfacial defects is suppressed, which together with suppression of surface-related recombination in thicker-shell structures leads to near-unity PL QYs in giant SQW NCs with the shell thickness greater than 4 nm.

In addition to high PL QYs, the property of practical importance for light-emitting applications is spectral tunability of emission. To examine the range of spectral tunability of giant SQW NCs ($R \approx 7.5$ nm), we have altered the dimensions of the CdS core, the CdSe emissive layer, and the final CdS shell and characterized optical properties of the resulting nanostructures. Figure 5 displays a progression of optical characteristics of CdS/CdSe/CdS SQW NCs with different geometries (r = 1.3, 1.5, or 1.9 nm, l = 0.3, 0.6, 0.8, 0.9, 1.2, or 1.5 nm, and $R \leq$ 7.5 nm). Regardless of the structure of the CdSe emissive layer, SQW NCs exhibit a similar shell thickness dependence of their optical properties. Namely, absorption and PL spectra gradually red shift with increasing CdS shell thickness (Figure 5a), and at the same time, the PL QY becomes progressively enhanced (Figure 5b). Smaller volume of the CdSe emissive layer results in the increase in the hole confinement energy, pushing the PL energy of giant SQW NCs ($R \approx 7.5$ nm) to 2.12 eV (Figure 5d). The changes in the CdS seed size and the thickness of CdSe emissive layer also affect the carrier confinement energy and the band gap of the giant SQW NCs (Figure 5c), yet the control over the volume of the CdSe emissive layer offers wider tunability of the PL energy (Figure 5d).

Figure 5e and Table 1 summarize optical properties of a series of giant SQW NCs with similar CdS shell thicknesses (h = 4.7−5.8 nm) and almost identical overall radii (R = 7.2−7.5 nm). This summary indicates that the majority of the samples (six out of seven) exhibit PL QYs in excess of 90%, in line with expectations that the SQW heterostructuring suppresses the formation of misfit defects even for very thick CdS shells. The only sample with a notably lower PL efficiency (~66%) is distinct from the others by much smaller volume of the CdSe emitting layer (8 nm^3 *versus* more than ~20 nm^3 in other samples). We propose at least two possible reasons for the observed reduction of the PL efficiency. One is a smaller electron−hole overlap compared to the other samples (0.17 *versus* more than 0.21), which slows down radiative recombination and thus makes the radiative recombination channel less competitive than nonradiative pathways involving carrier trapping (likely, hole trapping, as discussed earlier) at the CdS surface (Table 1 and Supporting Information). Another reason is that the latter process, which is mediated by tunneling, becomes more probable for a higher-energy hole state due to the reduced height of the tunneling barrier. It is noteworthy that the PL QY of 66% measured for the giant SQW NCs with a small CdSe volume is still much higher than that of giant CdSe/CdS C/S NCs with a similar PL energy (typically, the PL QYs of C/S NCs with peak PL emission at 600 nm are ~10% or less) and is comparable to the best PL QYs (~60%) of giant C/S NCs with similar shell thicknesses. The collection of PL QYs plotted in Figure 5f as a function of shell thickness highlights a considerable improvement in emission efficiencies of the SQW samples compared to more traditional giant C/S NCs. The disparity between the two types of samples is especially pronounced at larger shell thickness.

Light-emitting applications such as display, lightings, and lasers usually require concentrated NC assemblies.[2,4,7,8,10,12−17] Hence, understanding the optical properties of NCs in concentrated solution or dense films is essential to enhancing their performance in practical devices. To this end, we evaluated the concentration-dependent optical performances of CdS/CdSe/CdS giant SQW NCs prepared either as concentrated suspensions or solid-state films (Figure 5 and Figure S8, Supporting Information). In order to benchmark optical properties of the SQW NCs against those of other existing high-PL-QY NCs, we have also evaluated a series of reference samples with similar PL energies using the same conditions as those applied to the SQW samples. The reference NCs include type-I C/S CdSe (r = 2.0 nm)/$Cd_xZn_{1-x}S$ (h = 2.5 and 5.8 nm) structures and quasi-type-II C/S CdSe (r = 1.5 nm)/CdS (h = 2.0 and 6.0 nm) NCs; these two types of the samples are denoted as type I (R) and q-type II (R), respectively (Table 2).

We investigated the effect of concentration of NCs in solution by preparing solutions in various concentrations and film of densely packed NCs. The increase in the concentration of NCs in solution reduces the mean inter-NC distance, promotes aggregation and increases the chance for either

DOI: 10.1021/acsnano.6b03704
ACS Nano 2016, 10, 9297−9305

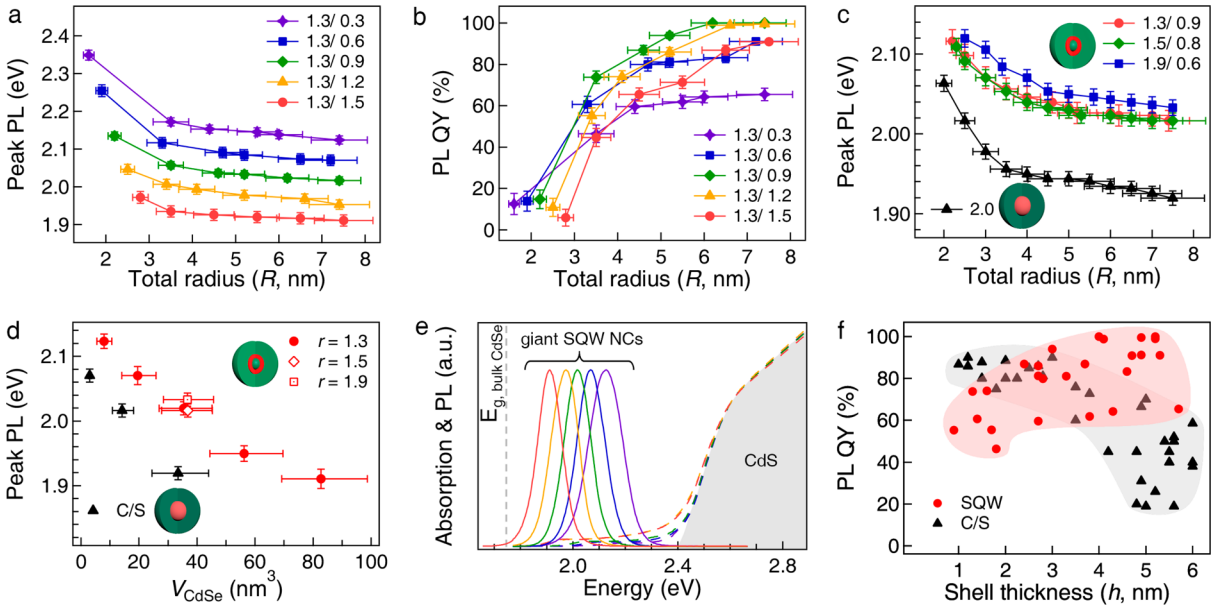

Figure 5. Optical properties of CdS/CdSe/CdS SQW NCs and CdSe/CdS C/S NCs with varying dimensions. (a) PL peaks in eV and (b) PL QYs of CdS (r = 1.3 nm)/CdSe (l = 0.3, 0.6, 0.9, 1.2, and 1.5 nm)/CdS NCs with varying shell thicknesses. (c) PL peaks in eV of CdS/CdSe/CdS SQW NCs with the same CdSe volume but different shell thicknesses (r/ l = 1.3/0.9 (circle), 1.5/0.8 (diamond), and 1.9/0.6 (square)). PL peaks in eV of CdSe (r = 2.0 nm)/CdS C/S NCs (triangle) are shown for comparison. (d) PL peaks in eV of giant CdSe/CdS NCs ($R \approx 7.5$ nm) and giant CdS/CdSe/CdS NCs ($R \approx 7.5$ nm) as a function of the volume of CdSe emissive layers. (e) Representative absorption and PL spectra of giant CdS/CdSe/CdS NCs ($R \approx 7.5$ nm). The gray shading in absorption represents the contribution of CdS. (f) PL QYs of CdSe/CdS C/S NCs and CdS/CdSe/CdS SQW NCs as a function of the exterior CdS shell thicknesses.

Table 1. Structural and Optical Properties of Giant SQW NCs with Varying Dimensions

$r/l/h$ (nm)	V_{CdSe} (nm^3)[a]	Θ_{e-h}[b]	peak PL (eV)	fwhm (meV)[c]	τ_r (ns)	PL QY (%)[d]
1.3/0.3/5.8	8.0	0.17	2.12	142	72	65.5
1.3/0.6/5.3	19.5	0.21	2.07	121	60	91.1
1.3/0.9/5.2	35.4	0.23	2.02	125	59	99.9
1.3/1.2/4.9	56.3	0.30	1.95	126	53	99.5
1.3/1.5/4.7	82.7	0.37	1.91	106	59	91.0
1.5/0.8/5.2	36.8	0.25	2.02	137	55	99.0
1.9/0.6/5.0	36.7	0.32	2.03	118	53	91.2

[a]Volume of the CdSe emissive layer determined by TEM analysis. [b]Electron−hole overlap integral. [c]Full width at half-maximum. [d]PL QYs measured using excitation wavelength of 450 nm.

Table 2. Optical Properties of CdS/CdSe/CdS (SQW) NCs, CdSe/Cd$_x$Zn$_{1-x}$S (type I) NCs, and CdSe/CdS (q-type II) NCs in Diluted Dispersion and in Film

		dispersion		film		
NC (R)	$\alpha_{abs/ems}$[a]	peak PL (eV)	PL QY (%)	peak PL (eV)	PL QY (%)	PL QY[b] (%, thermally annealed)
SQW (7.4)	35.6	2.02	99.9	1.94	63.3	63.0
type I (7.8)	8.1	1.99	89.8	1.90	50.4	49.0
type I (4.5)	12.3	1.96	82.9	1.86	35.5	28.4
q-type II (7.5)	63.0	1.96	58.7	1.91	40.7	39.8
q-type II (3.5)	7.7	2.03	88.6	1.94	37.3	18.7

[a]Ratio of optical density at the excitation energy (2.76 eV) and OD at 1S$_{e-h}$. [b]Room-temperature PL QY after exposure of film samples to 200 °C for 90 min.

radiative or nonradiative energy transfer (ET) between NCs. The red shift of the PL spectrum and the decrease in the PL QY are typical signatures of ET. We observed the smaller changes in the PL peak position and the PL QY in the q-type-II C/S NCs and the SQW NCs compared to the type-I samples (Figure 6a−e and Table 2). A thick shell keeps emissive layers further apart and thereby suppresses ET and subsequent red shift (Figure 6d,e and Table 2). Moreover, SQW NCs possess higher PL QY and thus are less affected by nonradiative recombination during the repeating ET steps. Due to their superior optical properties (high PL QY, small overlap between PL and absorption spectra, suppressed inter-NC ET, *etc.*), giant SQW NCs display PL QY higher than 80% in high-concentration solution (OD ∼ 40) and 60% in compact films, which exceed the values of conventional type-I or q-type-II C/S NCs by far. In addition to the high PL QY, the giant SQW NCs exhibit exceptional stability against heating (no detectable drop in the PL QY, Figure 6f), a critical feature required in thermal fabrication processes. We believe that the enhanced stability makes the SQW NCs more suitable in widely employed processing protocols for quantum-dot-based films.[51,52]

CONCLUSION

We have developed CdS/CdSe/CdS seed/spherical quantum well/shell NCs that exhibit exceptional optical properties and superior thermal stability. The highlight of the present work is that the giant SQW NCs exhibit near-unity PL QYs for CdS shell thicknesses greater than 5 nm. These structures are also characterized by a substantial suppression of single-NC PL blinking at room temperature. Spectroscopic studies along with a structural analysis suggest that, in these NCs, a thin CdSe emissive layer is coherently strained to fit the underlying lattice of the CdS seed, which allows for defect-free growth of the thick outer CdS shell. At sufficiently large shell thicknesses, hole tunneling to trap sites at the surface of the CdS shell becomes

DOI: 10.1021/acsnano.6b03704
ACS Nano 2016, 10, 9297−9305

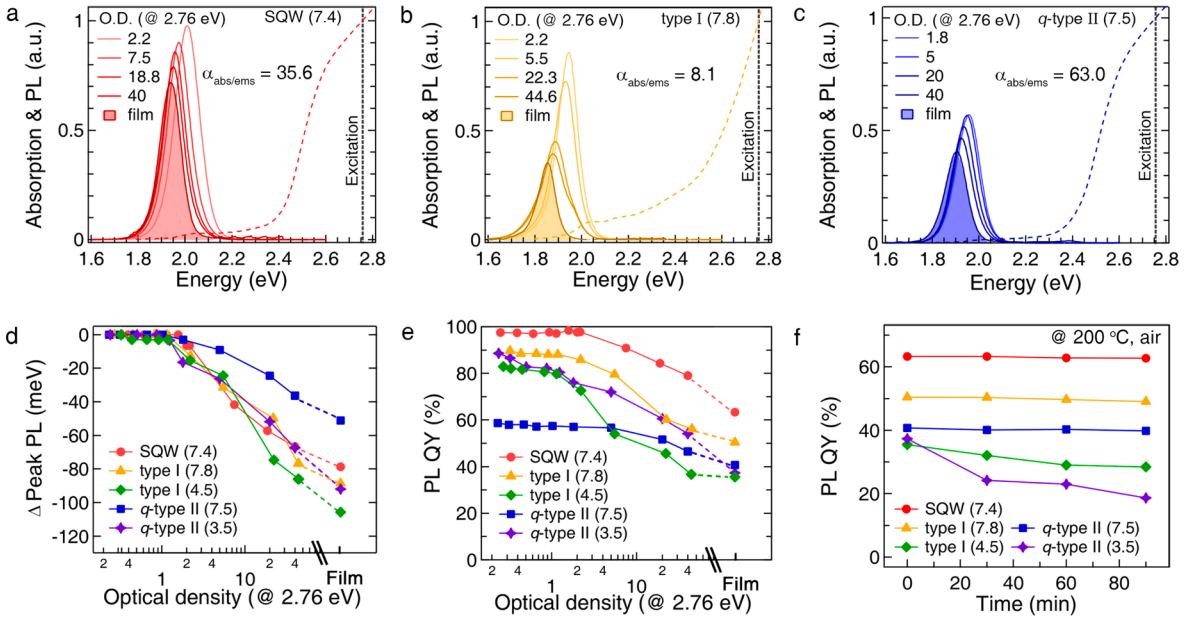

Figure 6. Concentration-dependent optical properties and thermal stability of CdS/CdSe/CdS SQW NCs. (a–c) Normalized absorption (dotted line) and PL spectra (solid line), (d) PL peak shift, and (e) PL QY of NC dispersions of varying concentrations (optical density at 450 nm) and films; $\alpha_{abs/ems}$ denotes a ratio of optical density at the excitation energy (2.76 eV) and optical density at $1S_{e-h}$. (f) PL QY of NC films as a function of exposure time to thermal stress (200 °C, air). CdS (r = 1.3 nm)/CdSe (l = 0.9 nm)/CdS (h = 5.2 nm), CdSe (r = 1.5 nm)/CdS (h = 2.0 and 6.0 nm), and CdSe (r = 2.0 nm)/$Cd_xZn_{1-x}S$ (h = 2.5 and 5.8 nm) are denoted as SQW, type I and q-type II with its total radius (R), respectively.

suppressed, which together with the suppressed formation of the misfit defects near the core/shell interface leads to nearly perfect PL QYs of around 100%. The systematic examination on the optical properties of the SQW NCs reveals that, in the spectral window of 1.91–2.12 eV, thick-shell SQW nanostructures systematically exhibit very strong light-emitting properties, which in some aspects are superior to those of more traditional thick-shell type-I and quasi-type-II C/S NCs. The superior performance of these nanostructures is especially pronounced in device-relevant dense assemblies of the NCs. The apparent next step is to examine the applicability of the proposed approach, SQW heterostructuring, to other types of NCs. We believe that the present study will inspire the materials research community to explore the ideas of SQW heterostructuring with other material combinations (*e.g.*, toxic-element-free III–V compositions), which will facilitate applications of colloidal NCs in real-life technologies including displays, lightings, and luminescent solar concentrators.

EXPERIMENTAL METHODS

Synthesis of CdS/CdSe/CdS Heterostructured NCs. Detailed synthetic methods and results are described in the Supporting Information. Heterostructured NCs were synthesized under Ar in a Schlenk line setup. CdO (99.95%, metals basis) and tri-*n*-octylphosphine (TOP, technical grade, 90%) were purchased from Alfa Aesar. Se (99.99%, powder), S (99.998%, powder), oleic acid (OA, 90%), 1-dodecanethiol (DDT, ≥98%), and 1-octadecene (ODE, 90%, technical grade) were purchased from Sigma-Aldrich. We prepared stock precursor solutions [0.5 M cadmium oleate ($Cd(OA)_2$) in ODE, 0.25 M sulfur dissolved in ODE (S-ODE), 0.5 M DDT in ODE; 2 M selenium in TOP (TOPSe), and 2 M sulfur in TOP (TOPS)] and stored them in a glovebox filled with Ar until use. For the synthesis of CdS (r = 1.3 nm)/CdSe/CdS NCs, CdO (0.3 mmol), OA (0.9 mmol), and ODE (10 mL) were loaded into a three-neck flask and heated to 270 °C under Ar to form a clear solution of $Cd(OA)_2$. CdS seeds were synthesized by injecting 0.25 M S-ODE (0.5 mL) into the reaction flask. After 10 min of reaction, the reaction flask was cooled to room temperature to complete the reaction. The resultant CdS seeds (r = 1.3 nm) were purified twice by the precipitation/redispersion method. For the growth of the CdSe emissive layer, the desired amount of mixed precursor solution (0.1 M $Cd(OA)_2$ and 0.1 M TOPSe diluted in ODE) was injected at a rate of 5 mL/h into the reaction flask that contained CdS seeds (0.1 g) and ODE (10 mL) at 300 °C under Ar. After the injection was completed, the reaction flask was maintained at the increased temperature for 10 min and then cooled to room temperature. The resulting CdS/CdSe NCs were purified twice. For CdS shelling, CdS (r = 1.3 nm)/CdSe (l = 0.9 nm) (0.1 g) and ODE (10 mL) were mixed in a flask and heated to 300 °C under Ar. At the temperature, the desired amounts of 0.5 M $Cd(OA)_2$ and 0.5 M DDT in ODE were injected separately into the reaction vessel at a rate of 2 mL/h. After the injection was completed, the reaction flask was maintained at the increased temperature for 30 min and cooled to room temperature. The synthesized NCs were purified and dissolved in nonpolar organic solvents for further characterization.

Optical and Structural Characterization. Absorption and PL spectra of NC solutions were obtained with a V-670 UV–visible/NIR spectrometer (Jasco) and a Fluoromax-4 spectrometer (Horiba). TEM images of NCs were taken with a JEOL 2010F microscope. The dimensions of various elements of the fabricated NCs (the core radius, the thickness of the emissive layer, the final shell thickness) were determined from HR-TEM images of reaction products at various stages of the synthesis. We calculated the average radius of nanocrystals and shell thickness from these measurements. Absolute PL QY of solution and film samples was measured at the excitation wavelengths (450 nm) with a QE-2100 (Otsuka Photal Electronics) equipped with an integrating hemisphere, a low stray light spectrometer, and fluorescent re-excitation elimination. For single-exciton decay dynamics measurement, the samples were excited at 450 nm (pulse width = 80 ps) at a repetition rate of 2.5 MHz, and PL dynamics were resolved using a time-correlated single-photon counting system that consists of avalanche photodiodes (temporal resolution = 350 ps) and a single channel analyzer (with a Picoquant Timeharp 260). The ON-time fraction is defined as the relative amount of time during which the single-dot PL intensity is equal to or

DOI: 10.1021/acsnano.6b03704
ACS Nano 2016, 10, 9297–9305

higher than the middle value between the two peaks, high- (bright) and low- (dark or gray) emissivity states, in the histogram of PL intensities.

The crystalline structures of NCs were investigated by synchrotron X-ray diffraction measurements at the 5A X-ray scattering beamline (X-ray wavelength = 1.54056 Å) at Pohang Accelerator Laboratory. The XRD data were acquired in the 2θ range between 10 and 130° at a scan rate of 0.05°/min. The XRD patterns of CdSe and CdS in CdS/CdSe NCs were decoupled by subtracting a separately measured XRD pattern of CdS NCs from that of CdS/CdSe NCs, with the volume of each component considered. For fabrication of the NC film, the NC layer was spun-cast from solution (20 mg/mL in hexane) at 2000 rpm for 30 s on a clean glass substrate (1.5 cm × 1.5 cm). The PL spectra and PL QY of NC films were characterized with the QE-2100.

ASSOCIATED CONTENT

Supporting Information

The Supporting Information is available free of charge on the ACS Publications website at DOI: 10.1021/acsnano.6b03704.

Detailed synthetic methods and characteristics of CdSe/CdS and CdSe/$Zn_xCd_{1-x}S$ C/S QDs (UV−vis spectra, PL spectra, PL decay dynamics, PL QYs, TEM images of NCs, and SEM images of NC films), XRD patterns of CdSe and CdSe/CdS C/S NCs, PL QY chart for CdSe/CdS (C/S) and CdS/CdSe/CdS (SQW) NCs, detailed calculation of critical thickness for NCs and electron−hole overlap integral for NCs (PDF)

AUTHOR INFORMATION

Corresponding Authors

*E-mail: pkw0818@ucla.edu.
*E-mail: dclee@kaist.edu.
*E-mail: wkbae@kist.re.kr.

Author Contributions

W.K.B. and B.G.J. conceived the idea. B.G.J. and J.H.C. synthesized NCs. Y.-S.P., V.I.K., and J.H.C. characterized and analyzed optical properties. I.C. and J.C. conducted NC film studies. W.K.B., D.C.L., and P.P. wrote the paper in consultation with all of the authors.

Notes

The authors declare no competing financial interest.

ACKNOWLEDGMENTS

This research was financially supported by Korea Institute of Science and Technology (KIST, 2E26530), the Ministry of Trade, Industry & Energy (MOTIE, 10051541) and Korea Display Research Consortium (KDRC) support program for the development of future devices technology for display industry. This work was supported from the National Research Foundation (NRF) grants funded by the Korean government (NRF-2014R1A2A2A01006739, NRF-2015R1A2A1A01004354, NRF-2016M3A7B4910618). Y.-S.P. and V.I.K. acknowledge the Chemical Sciences, Biosciences and Geosciences Division, Office of Basic Energy Sciences, Office of Science, U.S. Department of Energy.

REFERENCES

(1) Brus, L. Electronic Wave Functions in Semiconductor Clusters: Experiment and Theory. *J. Phys. Chem.* **1986**, *90*, 2555−2560.

(2) Colvin, V. L.; Schlamp, M. C.; Alivisatos, A. P. Light-Emitting Diodes Made from Cadmium Selenide Nanocrystals and a Semiconducting Polymer. *Nature* **1994**, *370*, 354−357.

(3) Kim, T.-H.; Cho, K.-S.; Lee, E. K.; Lee, S. J.; Chae, J.; Kim, J. W.; Kim, D. H.; Kwon, J.-Y.; Amaratunga, G.; Lee, S. Y.; Choi, B. L.; Kuk, Y.; Kim, J. M.; Kim, K. Full-Colour Quantum Dot Displays Fabricated by Transfer Printing. *Nat. Photonics* **2011**, *5*, 176−182.

(4) Kwak, J.; Bae, W. K.; Lee, D.; Park, I.; Lim, J.; Park, M.; Cho, H.; Woo, H.; Yoon, D. Y.; Char, K.; Lee, S.; Lee, C. Bright and Efficient Full-Color Colloidal Quantum Dot Light-Emitting Diodes Using an Inverted Device Structure. *Nano Lett.* **2012**, *12*, 2362−2366.

(5) Jun, S.; Jang, E. Bright and Stable Alloy Core/Multishell Quantum Dots. *Angew. Chem., Int. Ed.* **2013**, *52*, 679−682.

(6) Lim, J.; Park, M.; Bae, W. K.; Lee, D.; Lee, S.; Lee, C.; Char, K. Highly Efficient Cadmium-Free Quantum Dot Light-Emitting Diodes Enabled by the Direct Formation of Excitons within InP@ZnSeS Quantum Dots. *ACS Nano* **2013**, *7*, 9019−9026.

(7) Dai, X.; Zhang, Z.; Jin, Y.; Niu, Y.; Cao, H.; Liang, X.; Chen, L.; Wang, J.; Peng, X. Solution-Processed, High-Performance Light-Emitting Diodes Based on Quantum Dots. *Nature* **2014**, *515*, 96−99.

(8) Lim, J.; Jeong, B. G.; Park, M.; Kim, J. K.; Pietryga, J. M.; Park, Y.-S.; Klimov, V. I.; Lee, C.; Lee, D. C.; Bae, W. K. Influence of Shell Thickness on the Performance of Light-Emitting Devices Based on CdSe/$Zn_{1-X}Cd_XS$ Core/Shell Heterostructured Quantum Dots. *Adv. Mater.* **2014**, *26*, 8034−8040.

(9) Bae, W. K.; Lim, J.; Lee, D.; Park, M.; Lee, H.; Kwak, J.; Char, K.; Lee, C.; Lee, S. R/G/B/Natural White Light Thin Colloidal Quantum Dot-Based Light-Emitting Devices. *Adv. Mater.* **2014**, *26*, 6387−6393.

(10) Yang, Y.; Zheng, Y.; Cao, W.; Titov, A.; Hyvonen, J.; Manders, J. R.; Xue, J.; Holloway, P. H.; Qian, L. High-Efficiency Light-Emitting Devices Based on Quantum Dots with Tailored Nanostructures. *Nat. Photonics* **2015**, *9*, 259−266.

(11) Dang, C.; Lee, J.; Breen, C.; Steckel, J. S.; Coe-Sullivan, S.; Nurmikko, A. Red, Green and Blue Lasing Enabled by Single-Exciton Gain in Colloidal Quantum Dot Films. *Nat. Nanotechnol.* **2012**, *7*, 335−339.

(12) Park, Y.-S.; Bae, W. K.; Baker, T.; Lim, J.; Klimov, V. I. Effect of Auger Recombination on Lasing in Heterostructured Quantum Dots with Engineered Core/Shell Interfaces. *Nano Lett.* **2015**, *15*, 7319−7328.

(13) Klimov, V. I.; Schwarz, C. J.; McBranch, D. W.; Leatherdale, C. A.; Bawendi, M. G. Ultrafast Dynamics of Inter- and Intraband Transitions in Semiconductor Nanocrystals: Implications for Quantum-Dot Lasers. *Phys. Rev. B: Condens. Matter Mater. Phys.* **1999**, *60*, 2177−2180.

(14) Purcell-Milton, F.; Gun'ko, Y. K. Quantum Dots for Luminescent Solar Concentrators. *J. Mater. Chem.* **2012**, *22*, 16687−16697.

(15) Bronstein, N. D.; Li, L.; Xu, L.; Yao, Y.; Ferry, V. E.; Alivisatos, A. P.; Nuzzo, R. G. Luminescent Solar Concentration with Semiconductor Nanorods and Transfer-Printed Micro-Silicon Solar Cells. *ACS Nano* **2014**, *8*, 44−53.

(16) Coropceanu, I.; Bawendi, M. G. Core/Shell Quantum Dot Based Luminescent Solar Concentrators with Reduced Reabsorption and Enhanced Efficiency. *Nano Lett.* **2014**, *14*, 4097−4101.

(17) Meinardi, F.; Colombo, A.; Velizhanin, K. A.; Simonutti, R.; Lorenzon, M.; Beverina, L.; Viswanatha, R.; Klimov, V. I.; Brovelli, S. Large-Area Luminescent Solar Concentrators Based on`Stokes-Shift-Engineered' Nanocrystals in a Mass-Polymerized PMMA Matrix. *Nat. Photonics* **2014**, *8*, 392−399.

(18) Steigerwald, M. L.; Alivisatos, A. P.; Gibson, J. M.; Harris, T. D.; Kortan, R.; Muller, A. J.; Thayer, A. M.; Duncan, T. M.; Douglass, D. C.; Brus, L. E. Surface Derivatization and Isolation of Semiconductor Cluster Molecules. *J. Am. Chem. Soc.* **1988**, *110*, 3046−3050.

(19) Hassinen, A.; Moreels, I.; De Nolf, K.; Smet, P. F.; Martins, J. C.; Hens, Z. Short-Chain Alcohols Strip X-Type Ligands and Quench the Luminescence of PbSe and CdSe Quantum Dots, Acetonitrile Does Not. *J. Am. Chem. Soc.* **2012**, *134*, 20705−20712.

(20) Hines, M. A.; Guyot-Sionnest, P. Synthesis and Characterization of Strongly Luminescing ZnS-Capped CdSe Nanocrystals. *J. Phys. Chem.* **1996**, *100*, 468−471.

DOI: 10.1021/acsnano.6b03704
ACS Nano 2016, 10, 9297−9305

(21) Talapin, D. V.; Mekis, I.; Götzinger, S.; Kornowski, A.; Benson, O.; Weller, H. CdSe/CdS/ZnS and CdSe/ZnSe/ZnS Core−Shell−Shell Nanocrystals. *J. Phys. Chem. B* **2004**, *108*, 18826−18831.
(22) Xie, R.; Kolb, U.; Li, J.; Basché, T.; Mews, A. Synthesis and Characterization of Highly Luminescent CdSe−Core CdS/$Zn_{0.5}Cd_{0.5}S$/ZnS Multishell Nanocrystals. *J. Am. Chem. Soc.* **2005**, *127*, 7480−7488.
(23) García-Santamaría, F.; Chen, Y.; Vela, J.; Schaller, R. D.; Hollingsworth, J. A.; Klimov, V. I. Suppressed Auger Recombination in "Giant" Nanocrystals Boosts Optical Gain Performance. *Nano Lett.* **2009**, *9*, 3482−3488.
(24) Mahler, B.; Spinicelli, P.; Buil, S.; Quelin, X.; Hermier, J.-P.; Dubertret, B. Towards Non-Blinking Colloidal Quantum Dots. *Nat. Mater.* **2008**, *7*, 659−664.
(25) Malko, A. V.; Park, Y.-S.; Sampat, S.; Galland, C.; Vela, J.; Chen, Y.; Hollingsworth, J. A.; Klimov, V. I.; Htoon, H. Pump-Intensity- and Shell-Thickness-Dependent Evolution of Photoluminescence Blinking in Individual Core/Shell CdSe/CdS Nanocrystals. *Nano Lett.* **2011**, *11*, 5213−5218.
(26) Chen, Y.; Vela, J.; Htoon, H.; Casson, J. L.; Werder, D. J.; Bussian, D. A.; Klimov, V. I.; Hollingsworth, J. A. Giant" Multishell CdSe Nanocrystal Quantum Dots with Suppressed Blinking. *J. Am. Chem. Soc.* **2008**, *130*, 5026−5027.
(27) Chen, O.; Zhao, J.; Chauhan, V. P.; Cui, J.; Wong, C.; Harris, D. K.; Wei, H.; Han, H.-S.; Fukumura, D.; Jain, R. K.; Bawendi, M. G. Compact High-Quality CdSe−CdS Core−Shell Nanocrystals with Narrow Emission Linewidths and Suppressed Blinking. *Nat. Mater.* **2013**, *12*, 445−451.
(28) Canneson, D.; Biadala, L.; Buil, S.; Quélin, X.; Javaux, C.; Dubertret, B.; Hermier, J. P. Blinking Suppression and Biexcitonic Emission in Thick-Shell CdSe/CdS Nanocrystals at Cryogenic Temperature. *Phys. Rev. B: Condens. Matter Mater. Phys.* **2014**, *89*, 035303.
(29) Javaux, C.; Mahler, B.; Dubertret, B.; Shabaev, A.; Rodina, A. V.; Efros, Al. L.; Yakovlev, D. R.; Liu, F.; Bayer, M.; Camps, G.; Biadala, L.; Buil, S.; Quelin, X.; Hermier, J. P. Thermal Activation of Non-Radiative Auger Recombination in Charged Colloidal Nanocrystals. *Nat. Nanotechnol.* **2013**, *8*, 206−212.
(30) Spinicelli, P.; Buil, S.; Quélin, X.; Mahler, B.; Dubertret, B.; Hermier, J. P. Bright and Grey States in CdSe-CdS Nanocrystals Exhibiting Strongly Reduced Blinking. *Phys. Rev. Lett.* **2009**, *102*, 136801.
(31) Bae, W. K.; Padilha, L. A.; Park, Y.-S.; McDaniel, H.; Robel, I.; Pietryga, J. M.; Klimov, V. I. Controlled Alloying of the Core−Shell Interface in CdSe/CdS Quantum Dots for Suppression of Auger Recombination. *ACS Nano* **2013**, *7*, 3411−3419.
(32) Pal, B. N.; Ghosh, Y.; Brovelli, S.; Laocharoensuk, R.; Klimov, V. I.; Hollingsworth, J. A.; Htoon, H. 'Giant' CdSe/CdS Core/Shell Nanocrystal Quantum Dots As Efficient Electroluminescent Materials: Strong Influence of Shell Thickness on Light-Emitting Diode Performance. *Nano Lett.* **2012**, *12*, 331−336.
(33) Ghosh, Y.; Mangum, B. D.; Casson, J. L.; Williams, D. J.; Htoon, H.; Hollingsworth, J. A. New Insights into the Complexities of Shell Growth and the Strong Influence of Particle Volume in Nonblinking "Giant" Core/Shell Nanocrystal Quantum Dots. *J. Am. Chem. Soc.* **2012**, *134*, 9634−9643.
(34) Gong, K.; Kelley, D. F. Lattice Strain Limit for Uniform Shell Deposition in Zincblende CdSe/CdS Quantum Dots. *J. Phys. Chem. Lett.* **2015**, *6*, 1559−1562.
(35) Nasilowski, M.; Spinicelli, P.; Patriarche, G.; Dubertret, B. Gradient CdSe/CdS Quantum Dots with Room Temperature Biexciton Unity Quantum Yield. *Nano Lett.* **2015**, *15*, 3953−3958.
(36) Matthews, J. W.; Blakeslee, A. E. Defects in Epitaxial Multilayers. *J. Cryst. Growth* **1976**, *32*, 265−273.
(37) Battaglia, D.; Li, J. J.; Wang, Y.; Peng, X. Colloidal Two-Dimensional Systems: CdSe Quantum Shells and Wells. *Angew. Chem., Int. Ed.* **2003**, *42*, 5035−5039.
(38) García-Santamaría, F.; Brovelli, S.; Viswanatha, R.; Hollingsworth, J. A.; Htoon, H.; Crooker, S. A.; Klimov, V. I. Breakdown of Volume Scaling in Auger Recombination in CdSe/CdS Heteronanocrystals: The Role of the Core−Shell Interface. *Nano Lett.* **2011**, *11*, 687−693.
(39) Park, Y. S.; Malko, A. V.; Vela, J.; Chen, Y.; Ghosh, Y.; García-Santamaría, F.; Hollingsworth, J. A.; Klimov, V. I.; Htoon, H. Near-Unity Quantum Yields of Biexciton Emission from CdSe/CdS Nanocrystals Measured Using Single-Particle Spectroscopy. *Phys. Rev. Lett.* **2011**, *106*, 187401.
(40) Park, Y.-S.; Ghosh, Y.; Chen, Y.; Piryatinski, A.; Xu, P.; Mack, N. H.; Wang, H.-L.; Klimov, V. I.; Hollingsworth, J. A.; Htoon, H. Super-Poissonian Statistics of Photon Emission from Single CdSe-CdS Core-Shell Nanocrystals Coupled to Metal Nanostructures. *Phys. Rev. Lett.* **2013**, *110*, 117401.
(41) Zhao, J.; Chen, O.; Strasfeld, D. B.; Bawendi, M. G. Biexciton Quantum Yield Heterogeneities in Single CdSe (CdS) Core (Shell) Nanocrystals and Its Correlation to Exciton Blinking. *Nano Lett.* **2012**, *12*, 4477−4483.
(42) Galland, C.; Ghosh, Y.; Steinbruck, A.; Sykora, M.; Hollingsworth, J. A.; Klimov, V. I.; Htoon, H. Two Types of Luminescence Blinking Revealed by Spectroelectrochemistry of Single Quantum Dots. *Nature* **2011**, *479*, 203−207.
(43) Efros, A. L.; Rosen, M. Random Telegraph Signal in the Photoluminescence Intensity of a Single Quantum Dot. *Phys. Rev. Lett.* **1997**, *78*, 1110−1113.
(44) Brokmann, X.; Coolen, L.; Dahan, M.; Hermier, J. P. Measurement of the Radiative and Nonradiative Decay Rates of Single CdSe Nanocrystals through a Controlled Modification of Their Spontaneous Emission. *Phys. Rev. Lett.* **2004**, *93*, 107403.
(45) Gong, K.; Zeng, Y.; Kelley, D. F. Extinction Coefficients, Oscillator Strengths, and Radiative Lifetimes of CdSe, CdTe, and CdTe/CdSe Nanocrystals. *J. Phys. Chem. C* **2013**, *117*, 20268−20279.
(46) Espinobarro-Velazquez, D.; Leontiadou, M. A.; Page, R. C.; Califano, M.; O'Brien, P.; Binks, D. J. Effect of Chloride Passivation on Recombination Dynamics in CdTe Colloidal Quantum Dots. *ChemPhysChem* **2015**, *16*, 1239−1244.
(47) Qin, W.; Guyot-Sionnest, P. Evidence for the Role of Holes in Blinking: Negative and Oxidized CdSe/CdS Dots. *ACS Nano* **2012**, *6*, 9125−9132.
(48) Wei, H. H.-Y.; Evans, C. M.; Swartz, B. D.; Neukirch, A. J.; Young, J.; Prezhdo, O. V.; Krauss, T. D. Colloidal Semiconductor Quantum Dots with Tunable Surface Composition. *Nano Lett.* **2012**, *12*, 4465−4471.
(49) Matthews, J. W.; Blakeslee, A. E. Defects in Epitaxial Multilayers: I. Misfit Dislocations. *J. Cryst. Growth* **1974**, *27*, 118−125.
(50) Matthews, J. W.; Blakeslee, A. E. Defects in Epitaxial Multilayers: II. Dislocation Pile-Ups, Threading Dislocations, Slip Lines and Cracks. *J. Cryst. Growth* **1975**, *29*, 273−280.
(51) Jun, S.; Lee, J.; Jang, E. Highly Luminescent and Photostable Quantum Dot−Silica Monolith and Its Application to Light-Emitting Diodes. *ACS Nano* **2013**, *7*, 1472−1477.
(52) Coe-Sullivan, S.; Liu, W.; Allen, P.; Steckel, J. S. Quantum Dots for LED Downconversion in Display Applications. *ECS J. Solid State Sci. Technol.* **2013**, *2*, R3026−R3030.

DOI: 10.1021/acsnano.6b03704
ACS Nano 2016, 10, 9297−9305